Molecular and Electronic Structures of the Short-Lived Excited Triplet State of Tropone

Tadaaki Ikoma,* Kimio Akiyama, Shozo Tero-Kubota, and Yusaku Ikegami

Institute for Chemical Reaction Science, Tohoku University, Katahira 2-1-1, Aobaku, Sendai 980-8577, Japan

Received: July 1, 1997; In Final Form: October 31, 1997[⊗]

Time-resolved electron paramagnetic resonance experiments on the short-lived T_1 state of nonphosphorescent tropone were carried out using mixed crystals. Well-resolved hyperfine splittings due to allowed and forbidden transitions were observed at principal axes of the zero-field tensor. The spin density distribution, C−H bond angles, and the sign of the *D* value were deduced from the hyperfine spectra. It has been concluded that the T_1 state of tropone mainly has a $^3\pi\pi^*$ configuration and holds its molecular structure of C_{2v} symmetry. The experiments and molecular orbital calculations indicate that the large Franck−Condon factor between the T_1 and the S_0 states arises from the change of the potential surfaces due to the antibonding character of the π^* orbital at the C_4-C_5 bond in the T_1 state.

Introduction

Electron paramagnetic resonanc (EPR) spectroscopy has made a significant contribution to our understanding of the short-lived and nonphosphorescent lowest excited triplet (T_1) states. Time-resolved EPR (TREPR) and electron spin−echo spectroscopies have clarified that strong coupling between the close lying $^3n\pi^*$ and $^3\pi\pi^*$ states causes distortion of the potential surfaces of the T_1 states of diazaaromatic molecules[1] and pyridine,[2] resulting in the anomalous character of the phosphorescence. When the singly occupied orbital of the T_1 state has antibonding character, the triplet molecule often shows fast radiationless transition because of the different potential surfaces between the T_1 and S_0 states. In our previous papers,[3,4] we studied the magnetic properties and kinetics of the T_1 states of several troponoid compounds in glassy matrices by TREPR spectroscopy. Figure 1 shows the molecular structure of tropone. It has been found that the T_1 state of nonphosphorescent tropone has a very short lifetime of 5 μs at 4.2 K despite the pure $^3\pi\pi^*$ character. The fast nonradiative decay from the T_1 state has been interpreted by large Franck−Condon factor. The atomic coefficients of two unpaired orbitals (π_4 and π_5^*) are very different from each other in T_1 state tropone. Since the C_2-C_3 and C_4-C_5 bonds have an antibonding character in the π_5^* orbital, it can be deduced that the excitation into the T_1 state accompanies the increase of bond lengths or the twisting around these bonds. Thus, the detailed study on the molecular and electronic structures of the T_1 state is desirable in order to clarify the reason the Franck−Condon factor is so large. Hence, we have carried out the TREPR studies with some mixed crystals and molecular orbital (MO) calculations about T_1 state tropone.

In the present work, we observed the angular dependence of the TREPR spectra of T_1 state tropone doped in the single crystals of 1,4-dichlorobenzene and durene. At the stationary points, well-resolved hyperfine signals due to allowed ($\Delta m_I = 0$) and forbidden ($\Delta m_I \neq 0$) transitions were measured. From the analyses of the fine and hyperfine structures, we determined the zero-field splitting parameters and electron spin density distribution. The results suggest that the deviation from the planar structure is negligible in the T_1 state, but the bond length of C_4-C_5 is longer than that of the S_0 state. The origin of the fast radiationless transition from the T_1 state to the S_0 state has been discussed.

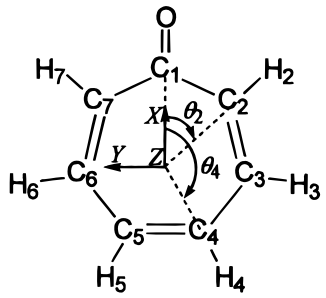

Figure 1. Molecular structure of tropone and its principal axes of fine structure tensor. θ_k is the angle between the C_2 axis and the C_k-H_k bond.

Basic Theory

The effective spin Hamiltonian ($\mathbf{H}_{eff}$) of triplet molecules consists of an electron Zeeman ($\mathbf{H}_{EZ}$), an electron spin−spin interaction ($\mathbf{H}_{SS}$), a nuclear Zeeman ($\mathbf{H}_{NZ}$), and a hyperfine interaction ($\mathbf{H}_{SI}$) as described by eq 1

$$\mathbf{H}_{eff} = \mathbf{H}_{EZ} + \mathbf{H}_{SS} + \mathbf{H}_{NZ} + \mathbf{H}_{SI}$$
$$= \mu_e \mathbf{S}\cdot\mathbf{g}_e\cdot\mathbf{B} + \mathbf{S}\cdot\mathbf{D}\cdot\mathbf{S} - \mu_n \sum_k \mathbf{I}^k\cdot\mathbf{g}_n^k\cdot\mathbf{B} + \sum_k \mathbf{S}\cdot\mathbf{A}^k\cdot\mathbf{I}^k \quad (1)$$

where the symbols have their usual meaning. In the present paper, a quadrupole interaction term is neglected because there is no nuclei with $I \geq 1$ in the case of tropone. Second-order perturbation treatments for $\mathbf{H}_{eff}$ were carried out for several special cases.[5−8] The general solution in an arbitrary coordination system by higher-order perturbation for the high-field case was given by Iwasaki.[9] The present work is also based on the high-field approximation condition: $\mathbf{H}_{EZ} > \mathbf{H}_{SS} \gg \mathbf{H}_{NZ}, \mathbf{H}_{SI}$.

[⊗] Abstract published in *Advance ACS Abstracts,* December 15, 1997.

S1089-5639(97)02115-4 CCC: $15.00
Published on Web 01/08/1998

Therefore, we can treat $\mathbf{H}_{\text{eff}}$ as two terms comprising an effective electron spin Hamiltonian ($\mathbf{H}_{\text{EZ}} + \mathbf{H}_{\text{SS}}$) and an effective nuclear spin Hamiltonian ($\mathbf{H}_{\text{NZ}} + \mathbf{H}_{\text{SI}}$).

The fine structure of an EPR spectrum can be interpreted in terms of the effective electron spin Hamiltonian. Assuming that $\mathbf{g}_e$ is isotropic, the matrix elements are presented by the zero-field spin functions (T_X, T_Y, T_Z) as follows.

$$\mathbf{H}_{\text{EZ}} + \mathbf{H}_{\text{SS}} = \begin{bmatrix} {}^1/_3D - E & \mu_e g_e B_Z & -i\mu_e g_e B_Y \\ \mu_e g_e B_Z & {}^1/_3D + E & \mu_e g_e B_X \\ i\mu_e g_e B_Y & \mu_e g_e B_X & -{}^2/_3D \end{bmatrix} \quad (2)$$

where D and E are zero-field splitting parameters and B_i is the external magnetic field component along the ith axis. The spectra of a randomly oriented sample and the angular dependence of the fine structure could be calculated from the above equation.

The observed hyperfine structure can be described by the effective nuclear spin Hamiltonian. On the basis of the high-field approximation and McConnell relation (Appendix A), these terms are given by the following simple formula.

$$\mathbf{H}_{\text{NZ}} + \mathbf{H}_{\text{SI}} = S_z \sum_k (\alpha_k I_z^k + \beta_k I_x^k + \gamma_k I_y^k) \quad (3)$$

For the notation of α, β, and γ, see eqs A5−A7 in the Appendix. k indicates a proton position. Forbidden transitions ($\Delta m_I \neq 0$) are induced by mixing among the nuclear spin sublevels due to the β and γ terms.

Experimental Section

Tropone was purified by distillation under reduced pressure. 1,4-Dichlorobenzene was purified by recrystallization followed by extensive zone refining. Recrystallized durene was passed through a column chromatograph on silica gel and then zone-refined extensively. The mixed single crystals were melt-grown by the Bridgman method in the dark. The initial concentration of guest tropone was 1−2 mol %, but the actual concentration of the guest in single crystals is considered to be less than 1 mol %. The crystals were cut to about 3 × 2 × 2 mm^3 size using the cleavage planes. The directions of the host crystal axes were identified with the aid of a polarizing microscope. The mixed crystals of 1,4-dichlorobenzene and durene were mounted on the sample holder so that the direction of the external magnetic field varied within the desired molecular plane of the guest molecule by rotating the holder. EPR measurements were performed at 10 K by using a variable temperature control unit of a helium cryostat (Oxford Model ESR 900). An excimer laser (Lumonics HD-300, injected XeCl gas (308 nm)) was used as the light pulse source. The TREPR system was described in a previous paper.[10]

Results and Discussion

Fine Structure. We first examined whether the tropone molecule homogeneously dissolved in host crystals without a thermal reaction during the crystal growth (80 °C, 72 h) by the Bridgman method. Figure 2d shows the randomly oriented TREPR spectrum obtained from the laser irradiation of the mixed polycrystalline of tropone and 1,4-dichlorobenzene prepared by the grind of the single crystal. The spectrum was observed at 500 ns after the laser pulse at 10 K. The spin polarization pattern of EAE/AEA indicates the preferential intersystem crossing to the middle sublevel, where E is emission and A is enhanced absorption of microwave, respectively. The zero-field parameters of $|D| = 0.077$ cm^{-1} and $|E| = 0.010$ cm^{-1} were determined by computer simulation (Figure 2e) on the basis of diagonalizing eq 2. The same polarization pattern and zero-field splitting parameters were obtained in the durene mixed crystal. The directions of the principal axes of the $\mathbf{H}_{\text{SS}}$ tensor were determined by magnetophotoselection experiments as shown in Figure 1.[3]

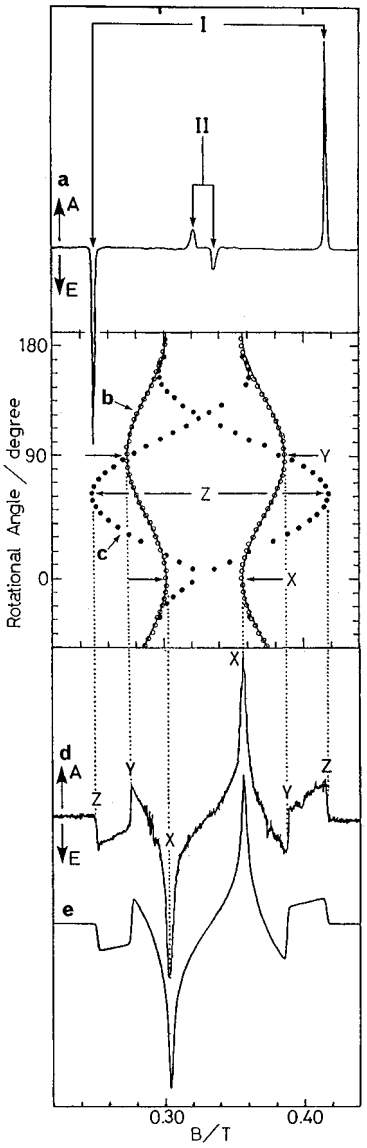

Figure 2. Time-resolved EPR spectra for the T_1 state of tropone doped in 1,4-dichlorobenzene single crystal (a) and its disordered system (d). The spectra (a and d) were measured at 500 ns after laser irradiation at 10 K. The angular dependence of fine structure in the oriented system is shown in b and c. Open (b) and closed (c) circles represent the magnetic fields of $|\Delta m_S| = 1$ resonances obtained when **B** rotated in the molecular plane of 1,4-dichlorobenzene, and in the plane with the in-plane short and out-of-plane axes of durene, respectively. The solid line in c and simulated spectrum (e) for d were calculated by using the parameters $|D| = 0.077$ cm^{-1}, $|E| = 0.010$ cm^{-1}, and $g_e = 2.003$.

Figure 2a is a typical TREPR spectrum of the T_1 state tropone observed in the 1,4-dichlorobenzene single crystal at 500 ns after laser pulse. Two kinds of signals due to magnetically different sites appeared. One site (I) shows the E/A pattern and the other site (II) indicates the A/E pattern from the low-field to high-field side. Figure 2b (open circles) depicts the angular dependence of the TREPR signals of tropone with the Zeeman field **B** rotating within the molecular plane of one of

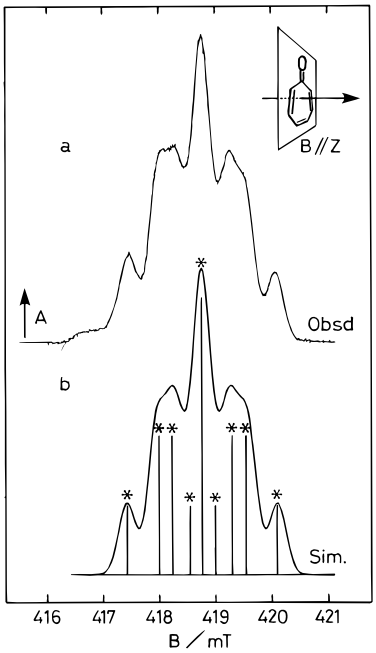

Figure 3. Hyperfine spectrum observed in a mixed crystal of durene at 10 K in **B** || *Z* (a) and simulation spectrum (b). Sticks specified by an asterisk in simulation spectrum are the allowed transitions.

the molecules in the unit cell of the 1,4-dichlorobenzene single crystal. Stationary points showing the minimum and maximum splittings completely coincide with the innermost (*X*) and intermediate (*Y*) canonical fields in the randomly oriented sample. The observed angular dependence of the signals is given by calculating with the same zero-field splitting parameters (solid lines).

Similarly the angular dependence of the TREPR signals of tropone was observed with the Zeeman field **B** rotating within the plane including the molecular normal axis (*Z*) as shown in Figure 2c (closed circles). These angular dependencies indicate that tropone is substituted in the manner that the carbonyl bond of tropone almost tended toward the direction of one of four methyl groups of host durene.

Hyperfine Structure. T_1 state TREPR spectra of tropone clearly showed the hyperfine structure in the $|\Delta m_S| = 1$ transitions at each of the canonical fields. A typical spectrum of the high-field side for **B** along the out of plane (*Z*) axis is shown in Figure 3a. The observed spectrum can be interpreted by the triplet of triplet hyperfine lines with an intensity ratio of 1:2:1, in which four protons are giving two different hyperfine splittings. As shown in Figure 3b, the spectrum was well reproduced by computer simulation, resulting in the proton hyperfine splitting constants of 0.815 and 0.515 mT, as well as the line width (a half-width at half-height, λ) of 0.180 mT of Gaussian type line shape. A weak signal appearing at the low-field side in Figure 3a is attributable to another triplet tropone in a different site in view of its angular dependence. The spectrum of the other $|\Delta m_S| = 1$ transition at 247.53 mT also exhibited the same hyperfine structure with all emissive polarization.

We carefully examined the angular dependence of the hyperfine splittings and the contribution of forbidden transitions to the hyperfine structure, but the results yielded no evidence for any deviation from the planar structure in T_1 state tropone within experimental error (±2°). Therefore, the T_1 state of tropone could be treated as a planar geometry for the analysis of the observed hyperfine structure in the present paper. According to the hyperfine structures measured at other orientations as shown in later, the hyperfine splittings of 0.815 and 0.515 mT can be assigned to 2,7- and 4,5-protons, respectively. The hyperfine splitting of 3,6-protons might be smaller than 0.1 mT judging from the line width. The above results clearly suggest that T_1 state tropone has C_{2v} symmetry and nearly planar structure.

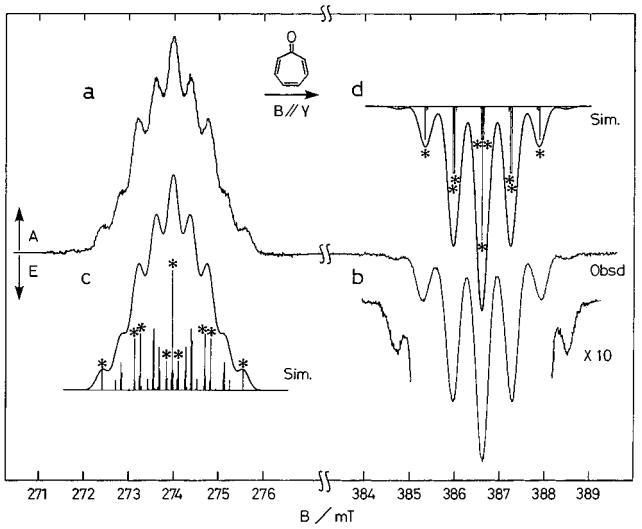

Figure 4. Hyperfine spectra observed in a mixed crystal of 1,4-dichlorobenzene at 10 K in **B** || *Y* (a and b) and simulation spectra (c and d). Sticks specified by an asterisk in simulation spectra are the allowed transitions.

When **B** is parallel to the *Y* axis, the hyperfine patterns observed at the low- and high-field region are quite different from each other as shown in Figure 4. The spectrum observed around 386.59 mT shows well-resolved quintet lines (1:4:6:4:1) with the hyperfine splitting of about 0.6 mT. The quintet lines are due to the hyperfine interactions with four protons at 2, 7, 4, and 5 positions. Very weak satellite lines are ascribable to the forbidden transitions according to their intensity and splitting. The low-field *Y* signals showed a very complicated hyperfine pattern, indicating the contribution of forbidden transitions as well as the allowed ones. The spectral feature reflects that the mixing degree of the nuclear spin multiple states in the $m_S = +1$ state is different from the $m_S = -1$ state. Since the hyperfine splitting constants of α-protons are generally negative in the π-electron system,[11−13] it is clear that the signals in high field and in low field correspond to the transitions from the $m_S = +1$ state to the $m_S = 0$ state and from the $m_S = -1$ state to the $m_S = 0$ state, respectively. This assignment leads to the conclusion that the sign of the *D* value of the T_1 state for tropone is positive.[14,15]

Figure 5 shows the hyperfine spectra in the low and high field in **B** || *X*. Although the hyperfine patterns are very similar to each other, the low-field signals show a slight broadening. This fact also suggests the role of EPR line widths from the forbidden transitions. The high-field spectrum can be interpreted tentatively by the triplet of triplet hyperfine lines with two kinds of hyperfine splittings (ca. 1 and 0.3 mT). The splittings are due to the 2,7- and 4,5-protons. The angular dependence of the hyperfine spectrum within the *XY* plane was symmetric about the *X* axis. This demonstrates that the *X* axis (||C═O) is a symmetric axis of the molecular structure for triplet state tropone.

We attempted to determine the hyperfine parameters, spin densities, and geometry in T_1 state tropone from the allowed and forbidden hyperfine spectra. As described above, the experiments indicate that T_1 state tropone has a planar structure

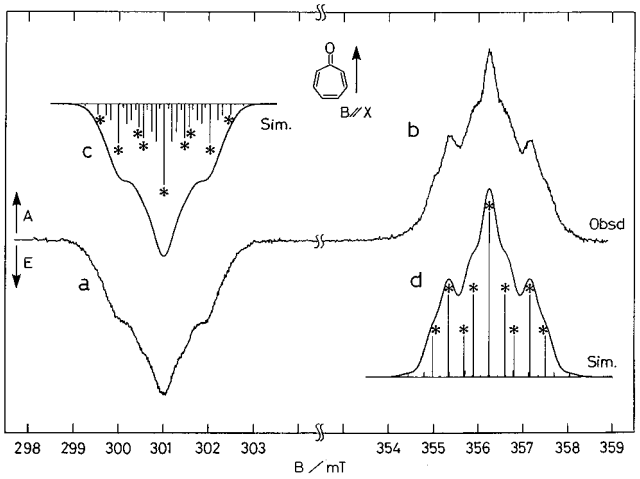

Figure 5. Hyperfine spectra observed in a mixed crystal of 1,4-dichlorobenzene at 10 K in **B** || *X* (a and b) and simulation spectra (c and d). Sticks specified by an asterisk in simulation spectrum are the allowed transitions.

TABLE 1: Principal Values (Q and A^d_{ii}, MHz) of the Hyperfine Tensor for α-Proton, π Spin Density (ρ_k) on the kth Carbon, and the Angle (θ_k, deg) between the C=O and C_k-H_k Bonds Estimated from the Simulation of the Hyperfine Spectra for the T_1 State of Tropone

Q	A^d_{LL}	A^d_{MM}	A^d_{NN}	$\rho_{2,7}$	$\rho_{4,5}$	$\rho_{3,6}{}^a$	$\rho_O{}^b$	$\theta_{2,7}$	$\theta_{4,5}$
−63.2	−4.7	39.6	−34.8	0.34	0.21	∼0.06	<0.4	53	150

[a] Determined from the line width of the Gaussian line in the spectrum **B** || *Z*. [b] Estimated by using the same hyperfine tensor elements as carbon and the same geometry as the S_0 state.

with C_{2v} symmetry. It can be expected that the precise analyses of the anisotropic hyperfine interaction would provide the values of the angles between the C_{2v} axis and C_k-H_k bond (θ_k). For the anisotropic hyperfine splittings due to 4,5-protons, only the dipolar interaction between the proton and the unpaired electron on the nearest-neighbor carbon atom was taken into account. On the other hand, it can be expected that for 2,7-protons the dipolar interaction with the electron spin on the carbonyl oxygen is also a relatively large contribution because of the short distance. To calculate the dipolar interaction between the 2,7-protons and the electron spin on the carbonyl oxygen, the geometry in the S_0 state was used.

Hyperfine spectrum can be simulated by diagonalizing eq 3 for the nuclear spin Hamiltonian. At first, we used the principal parameters of the hyperfine interaction of T_1 state benzene for the simulation. However, we could not obtain good reproduction of the hyperfine spectra. Thus, all the hyperfine parameters (Q, A^d_{LL}, A^d_{MM}, A^d_{NN}), spin densities (ρ_2, ρ_4, ρ_O), and the angles between the C_{2v} axis and C_k-H_k(θ_2, θ_4) were simultaneously optimized by the iterative simulation. From the simulation of the allowed transitions, we roughly determined these EPR and geometrical parameters. Then, we refined these parameters from the reproduction of the forbidden transitions because those are quite sensitive to the anisotropic elements of A^d_{LL} and A^d_{MM} as well as the values of θ_k.

The parameters obtained are summarized in Table 1. The principal values of the in-plane anisotropic interaction (A^d_{MM} and A^d_{NN}) are larger than the corresponding values of T_1 state benzene. The spin densities at the 2- and 4-positions of $\rho_2 = 0.34$ and $\rho_4 = 0.21$ were obtained. The spin density on the 3-position of $\rho_3 \sim 0.06$ was estimated from the anisotropic line width (λ) of the hyperfine spectra. When the spin density on the carbonyl oxygen, ρ_O, was larger than 0.4, significant deviation was obtained in the simulated spectrum from the observed one. Thus, the maximum value of ρ_O was determined. Since the spin density on C_1 dose not participate in any parameters, no information has been obtained from the experiments. The angle θ_k between the 2-fold axis and C_k-H_k bond were estimated. The angles of θ_2 and θ_7 are 53° and are the same as those in the S_0 state.[16] On the other hand, the angles of θ_4 and θ_5 are 150° which are smaller than those in the S_0 state. These facts strongly suggest the change of C_4-C_5 bond length as discussed below.

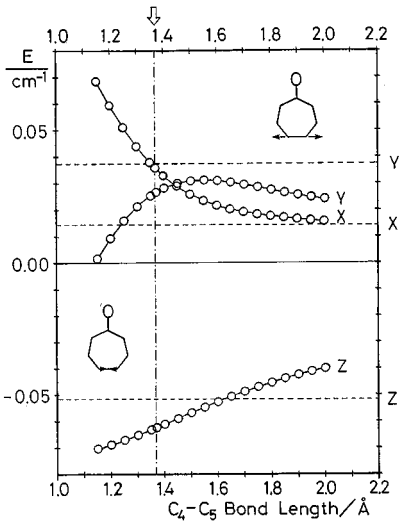

Figure 6. The calculated relative energies for three spin sublevels of the T_1 ($\pi_4\pi_5^*$) state plotted as a function of C_4-C_5 bond length. These energies were evaluated from the unpaired electron spin−spin interaction by using the SCF PPP-MOs, in which the configuration interaction was calculated with all configurations made by one electron excitation. The three horizontal lines (- - -) indicate the experimental principal values of spin sublevels. The vertical line (−•−) is the bond length of C_4-C_5 in the S_0 state.

Triplet Sublevels. The T_1 state of tropone has been assigned to be nearly pure $^3\pi\pi^*$ in character from the relatively small $|D|$ value and their small dependency on the matrix polarity.[3] Magnetophotoselection experiments have elucidated that the order of the sublevel energy is $T_Y > T_X > 0 > T_Z$. The present single-crystal experiments also support these facts. These results indicate that the energy level of the short axis T_Y sublevel is higher than that of the long axis T_X in tropone. This is unusual in the organic molecules with $^3\pi\pi^*$ character since the electron spin dipolar interaction mainly contributes to the energy levels of the triplet sublevels. Thus, we performed the molecular orbital calculations to clarify the structure dependence of the triplet sublevels. In tropone, the atomic coefficients of the lowest unoccupied molecular orbital (LUMO) (π_5^*) are very different from those of the highest occupied molecular orbital (HOMO) (π_4) and have relatively large values at C_2, C_4, C_5, and C_7 carbons.[3] Taking the antibonding character of the C_4-C_5 bond in the π_5^* orbital into the consideration, the excitation into the T_1 state would accompany the increase of this bond length. Since the electron spin dipolar interaction varies inversely as the cube of the distance between the unpaired electrons, the energy levels of the triplet sublevels are very sensitive to the bond length. Figure 6 depicts the C_4-C_5 bond length dependence of the sublevel energy levels. The energy levels due to the electron spin dipolar interaction were calculated by using the molecular orbitals obtained from SCF PPP method.[17] The spin−orbit coupling interaction was neglected because of the nearly pure $^3\pi\pi^*$ state. The energy level inversion for the T_Y and T_X sublevels was obtained at the bond

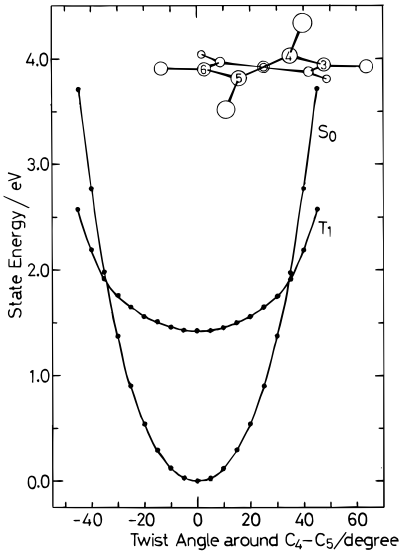

Figure 7. Energies of the S_0 and T_1 states plotted as a function of the dihedral angle between the $C_3-C_4-H_4$ and $C_6-C_5-H_5$ planes. The energies are calculated by the MNDO method in which all geometrical parameters except for the C_4-C_5 bond length were optimized at every point.

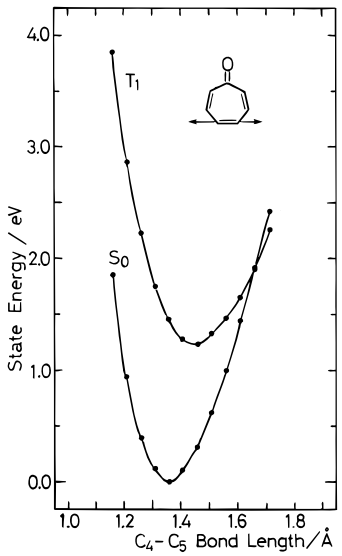

Figure 8. Energies of the S_0 and T_1 states plotted as a function of bond length between C_4 and C_5. The energies are calculated by the MNDO method in which all geometrical parameters were optimized at every point.

length of 1.44 Å. The order of the triplet sublevels is $T_Y > T_X > 0 > T_Z$ in the region of the longer C_4-C_5 bond lengths. It can be deduced from the calculations that the C_4-C_5 bond length is close to that of the single bond in T_1 state tropone. On the other hand, no good agreement was recognized in C_2-C_3 and C_6-C_7 bond length dependencies, in which both lengths changed simultaneously so as to keep a C_{2v} symmetry. The result agrees well with the geometry obtained from the experimental values of θ_4 and θ_5.

Nonradiative Decay. It has been clarified that the $^3\pi\pi^*$ state of tropone has very fast nonradiative decay from the triplet sublevels. Since there is no evidence for $^3n\pi^*-^3\pi\pi^*$ mixing, the short lifetime might be due to a large Franck−Condon factor induced by the difference of the potential surfaces between the T_1 and S_0 states. Therefore, the dependence of the potential surfaces on the molecular structure was also calculated. The calculations of the energies of these states were carried out by the MNDO method.[18] Figure 7 shows the state energy variations about the twisting angle around the C_4-C_5 bond. Here the C_4-C_5 bond length (1.35 Å) in the S_0 state was used. All other geometrical parameters were optimized in the S_0 state. The T_1 state as well as the S_0 state gives the energy minimum in the planar conformation. However, the calculation indicates that the potential surfaces in the T_1 state is shallower than that of the S_0 state. Tropone has 36 fundamental vibrational modes with the irreducible representations in the C_{2v} point group.[19] Out-of-plane vibrational modes with a_2 symmetry might correspond to this C_4-C_5 twisting coordinate of Figure 7. ν_{15} and ν_{18} normal modes, especially, are most probable as the promoting modes.

The C_4-C_5 bond length dependence of the potential surfaces was also calculated (Figure 8). The C_{2v} symmetry was kept in the calculations. The theoretical calculations indicate that the C_4-C_5 bond length is longer in the T_1 state than in the S_0 state by ca. 0.1 Å. The result is consistent with the conclusion obtained in the above section. We concluded, therefore, that the large Franck−Condon factor in the nonradiative decay is ascribable to the potential surface distortion and displacement in the T_1 which is caused by the antibonding character of the C_4-C_5 bond.

Conclusion

We have measured the TREPR spectra of the short-lived T_1 state of tropone in single crystals. Well-resolved hyperfine spectra were observed. The spectra were interpreted in terms of the effective spin Hamiltonian involving higher-order terms of hyperfine interaction. The appearance of forbidden transitions revealed that the sign of the D value of zero-field splitting parameters was positive. The estimated spin density distribution showed that the T_1 state is described with pure $\pi\pi^*$ configuration. The precise analysis of the hyperfine spectra leads to the conclusion that the excitation into the T_1 state induces the increase of the C_4-C_5 bond length, keeping the planar conformation with C_{2v} symmetry. The unusual order of the triplet sublevels was interpreted by the bond length change of C_4-C_5 bond. Semiempirical molecular orbital calculations clarified that the large Franck−Condon factor in the nonradiative decay from the T_1 state to the S_0 state is ascribable to the potential energy distortion and displacement in the T_1 state.

Appendix

Coordinate Transformations of Spin Systems and Hyperfine Interaction. We have to consider three different axis systems for Zeeman, zero-field, and hyperfine interactions in the effective spin Hamiltonian described in eq 1. An x,y,z axis system corresponds to the laboratory frame, where **B** is along the z axis. The principal axes of the fine tensor (X, Y, Z; see Figure 1) and hyperfine tensor (L, M, N; see Figure 9.) are based on the molecular coordinate.

The electron spin angular momentum is quantized by $\mathbf{H}_{EZ}$ and $\mathbf{H}_{SS}$. Within a limit of conventional high-field approximation ($\mathbf{H}_{EZ} > \mathbf{H}_{SS}$), the electron spin angular momentum vector is well represented by (S_x, S_y, S_z). For nuclear spin angular momentum, the local magnetic field from electron spins affects the quantization direction of nuclear spins. The electron and nuclear spin angular momenta are transformed from the principal

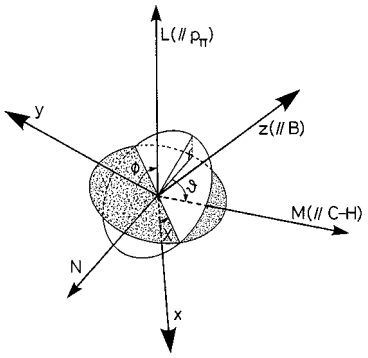

Figure 9. Two kinds of axes systems of hyperfine interaction (*L*, *M*, *N*) and laboratory frame (*x*, *y*, *z*). The *L* and *M* axes are parallel to the direction of singly occupied p_π orbital and to the directions of C−H bond, respectively. The *N* is perpendicular to both the *L* and *M* axes. The *z* axis is taken along the direction of external magnetic field **B**. The rotational angles between two systems are defined by the Euler angles (χ, ϕ, θ).

axis system of the hyperfine tensor into the laboratory frame.

$$\begin{bmatrix} S_L \\ S_M \\ S_N \end{bmatrix} = \mathbf{O} \cdot \begin{bmatrix} 0 \\ S_z \\ 0 \end{bmatrix} \tag{A1}$$

$$\begin{bmatrix} I_L \\ I_M \\ I_N \end{bmatrix} = \mathbf{O} \cdot \begin{bmatrix} I_y \\ I_z \\ I_x \end{bmatrix} \tag{A2}$$

$$\mathbf{O} = \begin{bmatrix} \cos\phi & \sin\phi\cos\chi & -\sin\phi\cos\chi \\ -\cos\theta\sin\phi & \cos\theta\cos\phi\cos\chi + \sin\theta\sin\chi & -\cos\theta\cos\phi\sin\chi + \sin\theta\cos\chi \\ \sin\theta\sin\phi & -\sin\theta\cos\phi\cos\chi + \cos\theta\sin\chi & \sin\theta\cos\phi\sin\chi + \cos\theta\cos\chi \end{bmatrix} \tag{A3}$$

where, **O** is the transformation matrix involving three Euler angles of χ, ϕ, and θ as shown in Figure 9. Here, the *x* and *y* components of electron spin are negligible because of the fast precessing motion of the electron spin along the *z* axis as compared with the nuclear motion.

The hyperfine tensor, **A**, consists of the isotropic and anisotropic terms. Both components are made up by summation of all interactions between all spin densities and protons. When the isotropic interaction is written by the McConnell equation that takes account of the interaction through only the C−H σ bond, the **A** tensor is reduced to the following formula[19]

$$\mathbf{A} = (Q^k\mathbf{U} + \mathbf{A}_k^d)\rho_k + \sum_{n\neq k}\mathbf{A}_k^d\rho_n = Q^k\mathbf{U}\rho_k + \sum_n \mathbf{A}_k^d\rho_n \tag{A4}$$

where **U** is unit matrix. Q_k and $\mathbf{A}_k^d$ are the isotropic hyperfine parameter and the anisotropic hyperfine tensor expected for unit spin population of a 2p orbital. All $\mathbf{A}^d$ tensors are diagonal and traceless. When the eqs A1, A2, and A4 are substituted into the hyperfine matrix, we obtain eq 3.

$$\mathbf{H}_{NZ} + \mathbf{H}_{SI} = S_z\sum_k(\alpha_k I_z^k + \beta_k I_x^k + \gamma_k I_y^k) \tag{3}$$

$$\begin{cases} \alpha_k = -\mu_n g_n B + \rho_k Q + \sum_n \rho_n (O_{21}^2 A_{LL}^d + O_{22}^2 A_{MM}^d + O_{23}^2 A_{LL}^d) & \text{(A5)} \\ \beta_k = \sum_n \rho_n (O_{31}O_{21}A_{LL}^d + O_{32}O_{22}A_{MM}^d + O_{33}O_{23}A_{LL}^d) & \text{(A6)} \\ \gamma_k = \sum_n \rho_n (O_{11}O_{21}A_{LL}^d + O_{12}O_{22}A_{MM}^d + O_{13}O_{23}A_{LL}^d) & \text{(A7)} \end{cases}$$

Assuming that the $\mathbf{A}_i^d$ of all fragments are equal to $\mathbf{A}^d$, the index *i* is removed.

Simulation Procedure. To simulate the fine structure spectra for the spin-polarized triplet state, the zero-field eigenfunctions $|T_X\rangle$, $|T_Y\rangle$, and $|T_Z\rangle$ were used as the basis set.

$$(|t_{+1}\rangle\ |t_0\rangle\ |t_{-1}\rangle) = (|T_X\rangle\ |T_Y\rangle\ |T_Z\rangle)\cdot\mathbf{C}_0 \tag{A8}$$

The $\mathbf{C}_0$ matrix is a function of the strength of |**B**| and the angle between **B** and *XYZ* system.

The diagonalization of the effective nuclear spin Hamiltonian matrix was also required to simulate the hyperfine spectrum. The three submatrices, $\langle t_i|\mathbf{H}_{NZ} + \mathbf{H}_{SI}|t_i\rangle$ were evaluated to create the effective nuclear spin Hamiltonian. The off-diagonal elements of $\langle t_i|\mathbf{H}_{NZ} + \mathbf{H}_{SI}|t_j\rangle$ were neglected. Then, those three submatices were separately diagonalized by using eight spin functions for four protons. The hyperfine splittings and relative intensity patterns were calculated from the eigenvalues and transition probabilities determined from nuclear spin eigenfunctions.

Acknowledgment. T.I. thanks Prof. N. Hirota of Kyoto University for his suggestion about forbidden transition. The present work was partially supported by grant-in-aid of Scientific Research on Priority Area No. 07404040 from the Japan Ministry of Education, Science and Culture.

References and Notes

(1) Hirota, N.; Yamauchi, S.; Terajima, M. *Rev. Chem. Intermed.* **1987**, *8*, 189.
(2) Buma, W. J.; Groenen, E. J. J.; Schmidt, J.; De Beer, R. *J. Chem. Phys.* **1989**, *91*, 6549.
(3) Ikoma, T.; Akiyama, K.; Tero-Kubota, S.; Ikegami, Y. *J. Phys. Chem.* **1991**, *95*, 7119.
(4) Ikoma, T.; Akiyama, K.; Tero-Kubota, S.; Ikegami, Y. *J. Phys. Chem.* **1993**, *97*, 303.
(5) Maruani, J.; Coope, J. A. R.; McDowell, C. A. *Mol. Phys.* **1970**, *18*, 165.
(6) Sakaguchi, U.; Arata, Y.; Fujiwara, S. *J. Magn. Reson.* **1973**, *9*, 118.
(7) Golding, R. M.; Tennant, W. C. *Mol. Phys.* **1973,** *25*, 1163.
(8) Rockenbauer, A.; Simon, P. *J. Magn. Reson.* **1973**, *11*, 217.
(9) Iwasaki, M. *J. Magn. Reson.* **1974**, *16*, 417.
(10) Ikoma, T.; Akiyama, K.; Tero-Kubota, S.; Ikegami, Y. *J. Phys. Chem.* **1989**, *93*, 7087.
(11) McConnell, H. M.; Heller, C.; Cole, T.; Fessenden, R. W. *J. Am. Chem. Soc.* **1960**, *82*, 766.
(12) Hirota, N.; Hutchison, C. A.; Palmer, P. *J. Chem. Phys.* **1964**, *40*, 3717.
(13) Clark, R. H.; Hutchison, C. A. *J. Chem. Phys.* **1971**, *54*, 2962.
(14) Vincent, J. S. *J. Chem. Phys.* **1971**, *54*, 2237.
(15) Iwasaki, M.; Minakata, K.; Toriyama, K. *J. Chem. Phys.* **1971**, *54*, 3225.
(16) Barrow, M. J.; Mills, O. S.; Filippini, G. *J. Chem. Soc., Chem. Commun.* **1973**, 66.
(17) Higuchi, J. *Bull. Chem. Soc. Jpn.* **1981**, *54*, 2864.
(18) MOPAC Ver. 5.00 (QCPE No. 445), Stewart, J. J. P. *QCPE Bull.* **1989**, *9*, 10. Hirano, T. *JCPE Newsletter* **1989**, *1*, 36. Revised as Ver. 5.01 by Toyoda, J. for Apple Machintosh.
(19) Redington, R. L.; Latimer, S. A.; Bock, C. L. *J. Phys. Chem.* **1990**, *94*, 163.
(20) Hutchison, C. A.; Nicholas, J. N.; Scott, G. W. *J. Chem. Phys.* **1970**, *53*, 1906.